JOURNAL OF PROPULSION AND POWER
Vol. 9, No. 4, July–Aug. 1993

Demonstration of Mode Transition in a Scramjet Combustor

G. A. Sullins*
Johns Hopkins University, Laurel, Maryland 20723

Direct-connect combustor hardware has been assembled at the Avery Propulsion Research Laboratory (APRL) of the Johns Hopkins University Applied Physics Laboratory (JHU/APL) to investigate a hydrogen-fueled scramjet combustor. The test hardware was designed to perform tests at simulated Mach 5 to Mach 8 flight conditions. This is done using a combustion heater with H_2 fuel and makeup O_2. The air, H_2 and O_2 flow rates are all supplied through computer-controlled digital valves. This system allows rapid changes in conditions and very steady flow rates can be maintained throughout the test. Recently, tests were performed in which the flow rates were systematically varied during the test to simulate an acceleration from $M = 5.9$ to 6.2. During this acceleration the fuel-air equivalence ratio was held constant and the combustor transitioned from a dual mode ramjet with a precombustion shock system creating subsonic flow at the injection plane, to a scramjet with no precombustion shock system. The results of these tests are presented along with descriptions of the hardware and control systems.

Nomenclature

A = area
ER = equivalence ratio
H = characteristic dimension for shock train correlation; typically the combustor height
M = Mach number
P = pressure
R_e = Reynolds number
S = shock train length
T = temperature
$\dot{w}$ = mass flow rate
γ = ratio of specific heats
θ = boundary-layer momentum thickness

Subscripts
t = stagnation
2 = isolator entrance condition
3 = combustor entrance conditions
4 = combustor exit condition

Introduction

IN developing high-speed vehicles utilizing air breathing propulsion systems, the desired cruising speed of the vehicle will determine the optimum cycle. Beyond Mach 3 flight speeds, the ramjet engine is the most efficient cycle[1] (see Fig. 1). In the $M = 3$–6 range, the ramjet operates most efficiently if the inlet diffuses the air to subsonic speeds. In the conventional ramjet (see Fig. 2a), the airflow is further decelerated to $M \approx 0.3$ by increasing the diffuser area; this ensures the complete combustion process will occur at subsonic speeds. A converging-diverging nozzle follows the combustor.

In the dual-mode ramjet (see Fig. 2b), the combustion process begins at subsonic speeds in a near constant area duct and continues through a diverging duct. The combustion process and area variation must be tailored to accelerate the flow from a subsonic to a sonic or supersonic speed at the combustor exit. (Sonic or supersonic speeds at the combustor exit are necessary due to the absence of a geometric throat). A diverging nozzle typically follows the combustor.

For the conventional ramjet, the shock system must be positioned at a location in the diffuser so as to maintain a sonic condition at the nozzle throat. Without a variable-

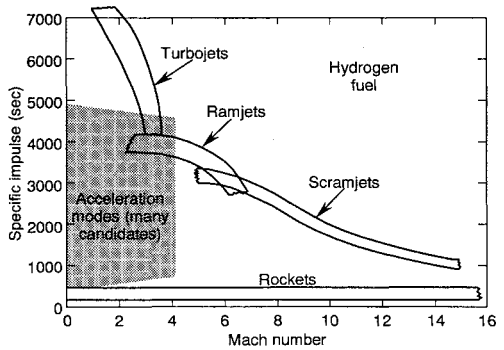

Fig. 1 Performance of hydrogen-fueled engines.

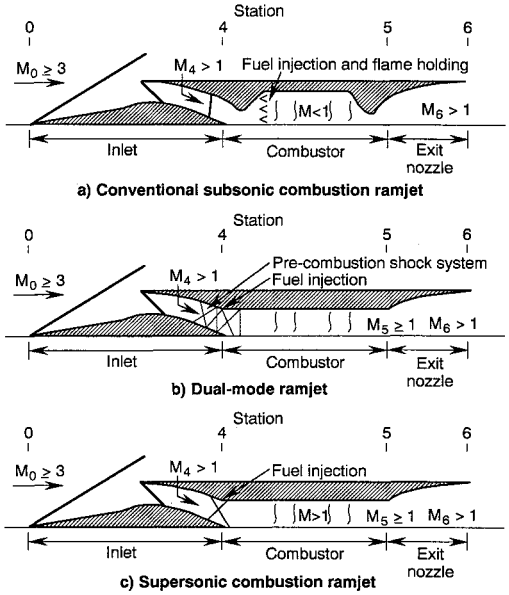

Fig. 2 Schematic of generic ramjet engines.

Received Jan. 2, 1991; revision received Nov. 30, 1992; accepted for publication Dec. 11, 1992.

*Principal Staff Engineer, Applied Physics Laboratory. Senior Member AIAA.

geometry nozzle, the conventional ramjet can only operate efficiently over a relatively narrow speed and altitude range. Since the dual-mode ramjet does not have the constraint of a geometric throat, it is a more optimum cycle if a wider operating range is required.

Above Mach 6–7 flight speeds, the total pressure loss resulting from the diffusion of the gas to subsonic speeds becomes excessive. Therefore, diffusing the air and completing the fuel-air mixing and reaction at supersonic speeds is advantageous (see Fig. 2c).

If the goal is to reach speeds where the supersonic combustion ramjet (scramjet) is appropriate, one approach is to utilize a propulsion system which accelerates the vehicle to $M \approx 3$ using one of several possible cycles (rocket, turbojet, etc.). At $M \approx 3$, a ramjet would take over and the combustor would operate in a dual mode to accelerate the vehicle to $M = 6$–7, where the cycle would transition to a pure scramjet.

In the dual-mode ramjet operation, the air leaves the inlet at supersonic speeds in the absence of combustion. The combustion of the fuel, however, causes a rapid increase in the pressure. Depending on the fuel flow rate, the entrance Mach number, and the combustor geometry, this pressure rise can surpass a level which the boundary layer can support, and separation occurs. The pressure feeds upstream of the fuel injectors, and a precombustion shock system is formed. This precombustion shock system can be of sufficient strength to create subsonic velocities at the combustor entrance, in fact this pressure ratio can be nearly equivalent in strength to that of a normal shock wave. The combustor geometry must therefore be designed in such a way that the combustion process accelerates the gas to a sonic or supersonic speed at the combustor exit.

In the inviscid limit, this shock system would be a single normal shock wave; however, due to the viscous boundary layer, this shock system is spread into a series of oblique or lambda shock waves depending on the boundary-layer thickness (see Figs. 3a and 3b). Stabilizing this shock system is important to avoid its interaction with the inlet. One method of doing this is to place a length of duct between the combustor and inlet, designated as an isolator, which is of sufficient length to accommodate the entire precombustion shock train. The determination of this length has been the topic of several studies.[2–4] For a given ER, the length of this shock train decreases as the vehicle accelerates, which can be seen in the following example.

The total temperature rise across the combustor can be approximated by[5]

$$(T_{t4}/T_{t3}) = 1 + ER[(4500/T_{t3}) - 0.3] \quad (1)$$

this equation is based on a curve fit of results from an equilibrium chemistry analysis of hydrogen and air. At a typical

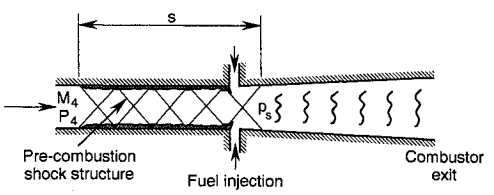

Fig. 3a Shock train with oblique waves due to thin incoming boundary layer.

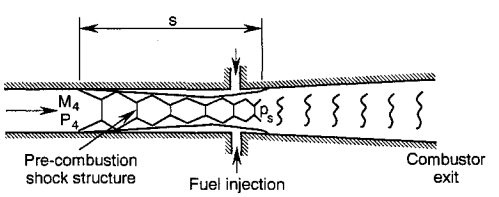

Fig. 3b Shock train with lambda shock waves due to thick incoming boundary layer.

Mach 4 flight condition, the stagnation temperature at the combustor entrance is $T_{t3} \approx 1640$°R, assuming $\gamma = 1.4$ and no inlet thermal losses. For a stoichiometric equivalence ratio ($ER = 1$), the total temperature rise across the combustor is therefore

$$(T_{t4}/T_{t3}) = 3.44 \quad (2)$$

At a Mach 5 flight condition, the combustor entrance condition increases to $T_{t3} \approx 2340$°R, and therefore, the temperature rise across the combustor, for an $ER = 1$, is reduced to

$$(T_{t4}/T_{t3}) = 2.62 \quad (3)$$

The result is, for a constant ER, the relative pressure rise produced in the combustor is reduced as the vehicle accelerates, and a weaker precombustion shock system is required.

The length of the shock train S has been shown to be a function of its strength (P_3/P_2), the incoming Mach number (M_2), and θ[2–4]

$$S = \frac{2\sqrt{H\theta}}{(M_2^2 - 1)Re_\theta^{0.25}}\left[50\left(\frac{P_3}{P_2} - 1\right) + 170\left(\frac{P_3}{P_2} - 1\right)^2\right] \quad (4)$$

As the vehicle accelerates, M_2 increases and the shock strength (P_3/P_2) decreases, resulting in a shorter shock train length.

At some speed in the trajectory, generally in the $M = 6$–8 speed regime, a transition occurs where this shock system weakens to the point that the average speed of the flow is supersonic at the combustor entrance and the engine operates as a scramjet. At this point the precombustion shock system is still of significant strength, but is weaker than a normal shock. As the vehicle accelerates further, the strength of the shock decreases to the point that the pressure rise is less than the boundary-layer separation pressure ratio and the shock system is swallowed. The transition of the precombustion shock system from near normal shock strength to its elimination occurs between $M = 5$ and $M = 8$, depending on the engine geometry and the fuel flow schedule. In this article, the portion of the transition in which the shock system is eliminated is addressed.

A direct-connect hydrogen fueled scramjet combustor facility was established at the APRL of JHU/APL. The goal of the test program was to extend the existing data base on hydrogen fueled scramjet combustors. As part of this program, tests were performed to simulate a vehicle acceleration from $M = 5.9$ to 6.2 by varying the combustor entrance stagnation temperature. A precombustion shock system of significant strength ($P_3/P_2 \approx 6$) was initially established upstream of the injectors; however, during the simulated acceleration, this shock system was eliminated. A description of the hardware used for these tests is presented along with the results of the tests.

Experimental Apparatus

Figure 4 is a schematic diagram of the direct-connect scramjet combustor test setup used at JHU/APL. A combustion heater with hydrogen fuel, and makeup oxygen, is used to heat the air to Mach 5–8 flight enthalpies. The gas is accelerated through a $M = 3.3$ supply nozzle prior to entering the scramjet combustor. The heater, nozzle, and combustor are mounted on a thrust stand. Downstream of the combustor, the exhaust duct is decoupled from the thrust stand at the combustor exit, using a slip fitting made of viton.

A total of 365 instruments are used to determine combustor performance. These include wall static pressures, instream pitot pressures, thermocouples, heat flux calorimeters, flowmeters and a thrust stand.

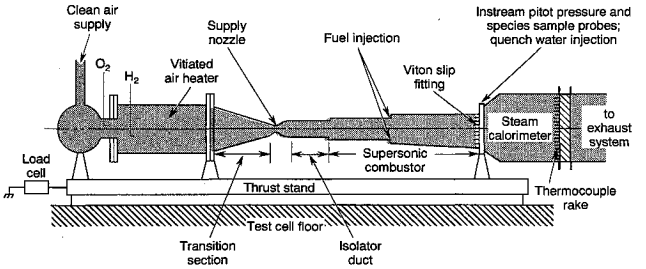

Fig. 4 Schematic of test setup.

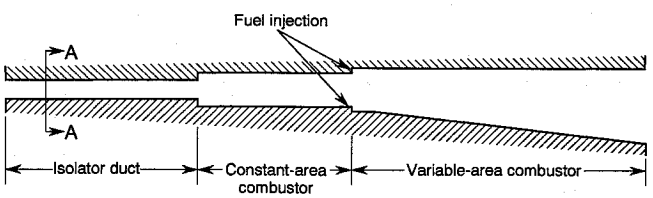

Fig. 5 Schematic of Applied Physics Laboratory scramjet combustor.

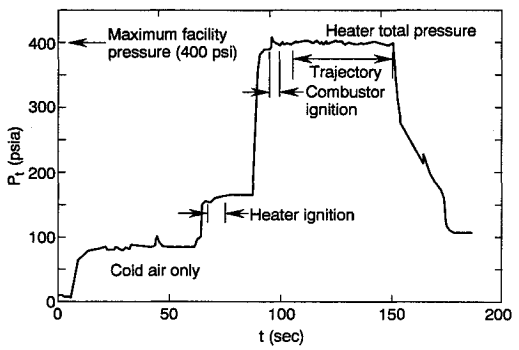

Fig. 6 Pressure in the combustion heater during the simulated vehicle acceleration test.

The combustor cross section is of rectangular shape and is fabricated of thick nickel plates clamped together. This simple design allows for easy configuration changes and a rapid repair should a section be damaged during a test. The combustor consists of three sections (see Fig. 5): 1) an isolator duct, 2) a constant area combustor, and 3) a variable area combustor.

The hardware has the capability to inject fuel at various axial locations. For the results presented here, the fuel was injected at the exit of the constant area combustor (see Fig. 5) through instream fuel injectors. This was done because higher fuel flow rates (up to stoichiometric fuel-air ratios; $ER = 1$) could be tested using the aft fuel injector location. By doing this, the constant area combustor section was used as additional isolator duct length. This constant area combustor section and the upstream fuel injection station are primarily used at higher flight Mach numbers ($M > 7$).

The hardware is a heat-sink design (i.e., uncooled). The drawback in using uncooled hardware is that the test time is limited ($t \leq 60$ s) to avoid thermal damage. The advantage is the simplicity and the freedom of instrumentation placement. The high conductivity of the nickel allows heat conduction away from "hot spots" to help prevent damage. A zirconia coating (0.020-in. thick) was placed on the inner wall surface. Zirconia (ZrO_2) is a ceramic material with a low thermal conductivity and a very high melting temperature, thereby providing a thermal protection for the nickel.

Since the test time is limited, reaching steady-state flow rates of the gases rapidly is essential. This is achieved through the use of computer-controlled digital valves for the air, hydrogen, and oxygen supplies. The rapid switching of these valves coupled with the computer control allows the valves to maintain a steady pressure in the heater (typically within $\pm 1\%$) throughout the test (see Fig. 6). For this test, the program was set to vary the flow rates of hydrogen, air, and oxygen to simulate a vehicle acceleration. All three valves are driven by a single Hewlett-Packard series 200 engineering work station using HP Technical Basic. The computer program has a "quick point" algorithm which allows a rapid transition from one operating point to another. This is illustrated in Fig. 6, where the heater total pressure and temperature were changed from $P_t = 175$ psi and $T_t = 1000$°R (the heater ignition condition) to $P_t = 400$ psi and $T_t = 2700$°R (the desired operating pressure) in approximately 3 s. The heater pressure was then maintained at a constant value of 400 psi for 60 s as the heater total temperature was increased from $T = 2700°$ to 3070°R.

Results and Discussion

As previously mentioned, a combustion heater was used to heat the supply air. The fuel-air ratio required to produce several temperatures are shown in Fig. 7. The simulated flight Mach number of each of these temperatures is also indicated in Fig. 7. The intent of this test series was to attempt to vary the temperature from $T_t = 2560$°R (simulated $M = 5.7$ flight condition based on total enthalpy) to $T_t = 3070$°R (simulated $M = 6.2$ flight condition). Though a much wider range was possible, this variation over 45 s was felt to approximate a reasonable vehicle acceleration. Furthermore, steady-state tests in this flight speed regime produced a dramatic change in the shock structure when an equivalence ratio of $ER = 0.6$ was used.

One goal of the tests was to determine if the transient operation of the combustor compared favorably with the steady-state operation. In order to check this, a test was run at both end points, $T_t = 2560$°R and $T_t = 3070$°R (see Fig. 7). Several fuel flow rates were tested ($0.5 < ER < 1$) at each simulated Mach number. While the combustor could operate at a stoichiometric condition without a combustor unstart (i.e., forcing the precombustion shock system into the inlet) the results did not indicate that a mode transition would occur for an $ER > 0.6$ in this speed regime. It is important to point out that in a vehicle it is typically desirable to operate the engine at the maximum equivalence ratio ($ER = 1$) in order to accelerate the vehicle to its cruising speed as quickly as possible. This demonstration, could have been performed at an $ER = 1$; however, the transition would have occurred at a higher Mach number and it would have required additional tests to find the transition point. Therefore, due to time constraints, an $ER = 0.6$ was chosen. There is no reason to believe that the results at $ER = 1$ would be different than those tested here.

The measured pressure on the combustor lower wall is plotted for the steady-state tests (see Fig. 8). A significant change in the combustor operation occurs between the two simulated flight conditions. For the simulated $M = 5.7$ condition ($T_t = 2560$°R), the pressure in the combustor reaches $P \approx 47$ psia,

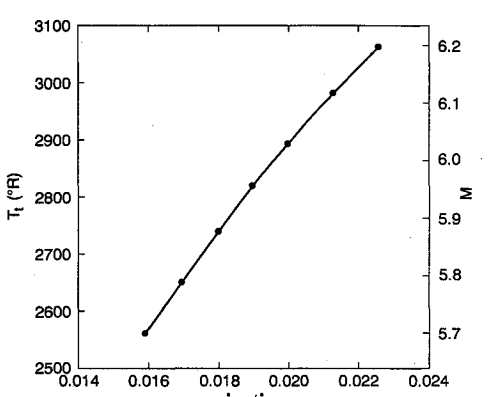

Fig. 7 Mode transition demonstration—pretest predictions.

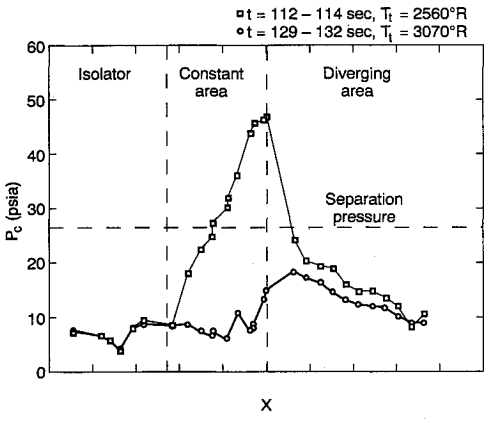

Fig. 8 Lower wall pressure traces for steady-state operation.

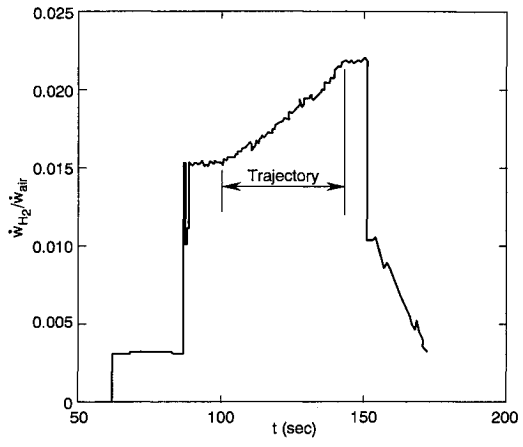

Fig. 9 Fuel-air ratio is increased to simulate acceleration.

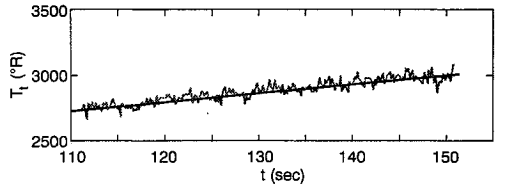

Fig. 10 Measured total temperature during simulated acceleration.

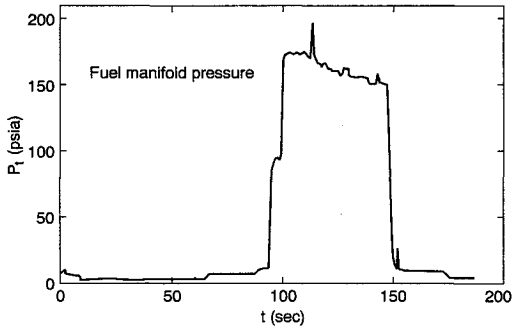

Fig. 11 Combustor fuel manifold pressure.

which is well above the separation pressure ($P_{sep} \approx 27$ psia for these test conditions). This causes a precombustion shock train to form upstream of the injectors, resulting in subsonic flow ($M \approx 0.7$) at the injection station. This shock train pressure rise is equivalent to 60% of that due to a normal shock wave. At the $M = 6.2$ condition ($T_t = 3070$°R) the pressure reaches $P \approx 22$ psia which is below the separation pressure. The result is supersonic flow throughout the combustor. There was a concern, that once a strong precombustion shock system and separated region was established, it would remain for the second condition. In order to avoid this, the combustor fuel flow rate was reduced to a piloting condition ($ER = 0.3$) between operating points ($T_t = 2560$°R and $T_t = 3070$°R) to obtain a steady-state baseline.

The curve from Fig. 7 was used to determine the required flow rates of air, hydrogen, and oxygen to simulate an acceleration. Figure 9 shows the actual hydrogen-to-air ratio delivered to the heater. This ratio is increased by simultaneously increasing the hydrogen and decreasing the airflow. At $t \approx 100$ s, the trajectory was initiated and a near linear variation was attained for 45 s. According to the pretest prediction (Fig. 7), this should have produced a stagnation temperature variation from $T_t = 2560$–3070°R. A platinum/platinum 13% rhodium thermocouple was positioned instream, approximately 3-in. downstream of the supply nozzle. The measured temperature is shown vs time (see Fig. 10) for the trajectory portion of the test; also shown in Fig. 10, is a first-order polynomial fit of the data. As can be seen, the temperature rise was linear as planned; however, the temperature appears to have started at $T_t = 2720$°R rather than the desired $T_t = 2560$°R. This was due to the actual heat loss in the heater and nozzle being less than had been anticipated. The total temperature did, however, reach $T_t = 3070$°R at the end of the trajectory. Referring again to Fig. 7, the simulated flight condition based on the thermocouple measurement was actually $M = 5.85$–6.2.

The heater total pressure vs time for the entire test was shown in Fig. 6. Heater ignition occurred at $t \approx 70$ s; final checks of several parameters (primarily water flow rates) are made at this relatively benign condition ($P_t \approx 175$ psi and $T_t \approx 1000$°R). At $t \approx 88$ s the heater was taken to its operating pressure ($P_t = 400$ psi). This is the maximum operating pressure due to structural constraints on the existing supply nozzle. The entire trajectory simulation was performed at the maximum pressure, as can be seen in Fig. 6.

As previously mentioned, in order to increase the total temperature while maintaining a constant total pressure, requires increasing the H_2 and O_2 flow rates while simultaneously decreasing the air flow rate. Therefore, to maintain a constant equivalence ratio in the combustor during the acceleration, the fuel flow rate was steadily decreased. The combustor fuel manifold pressure is shown in Fig. 11. At $t = 93$ s the fuel flow was started to the combustor at a "light off" condition ($ER \approx 0.38$). At $t = 100$ s the fuel flow rate was increased to the desired condition ($ER = 0.6$) and the trajectory began at $t \approx 110$ s. A pressure spike occurred shortly after the fuel flow began to decrease ($t \approx 114$ s), this pressure rise affects the entire combustor operation as will be seen in several subsequent plots. A much smaller fuel flow abnormality occurred at $t \approx 127$ s. For the most part, the fuel flow rate decreased at a linear rate, thus providing a constant equivalence ratio.

Wall static pressure traces at four axial locations within the combustor are shown in Fig. 12. The first trace (Fig. 12a) is well upstream of the fuel injection station. At $t \approx 90$ s the heater was at its operating condition and the pressure was $P = 10$ psia. As the fuel flow rate was increased ($t = 100$ s), the pressure increased significantly, indicating the presence of a precombustion shock system. A pressure spike is seen at $t = 114$ s, corresponding to the fuel increase. At $t = 116$ s the pressure began to decrease indicating that the leading edge of the shock system was moving downstream. For $t > 120$ s the pressure is equal to that for no fuel, indicating that the shock systems was completely downstream of this station.

Figure 12b is a pressure trace further downstream, but still upstream, of the injection station. This trace shows a more transient behavior than the first. Again, the fuel surge at $t = 114$ s caused a pressure spike. The same pressure reduction trend is observed for $t > 116$ s, indicating that the shock system

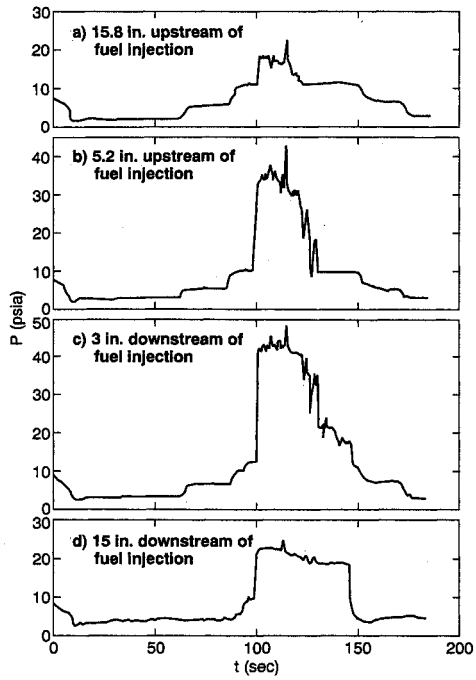

Fig. 12 Combustor pressure traces during transition.

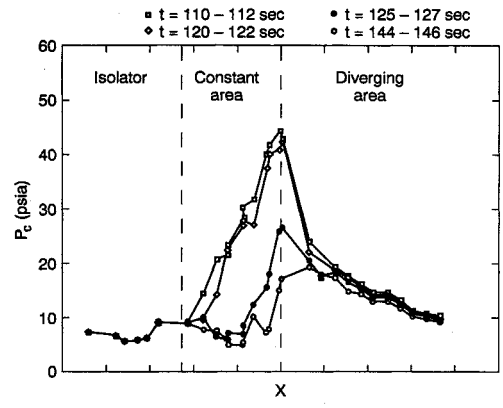

Fig. 13 Lower wall pressure traces during mode transition.

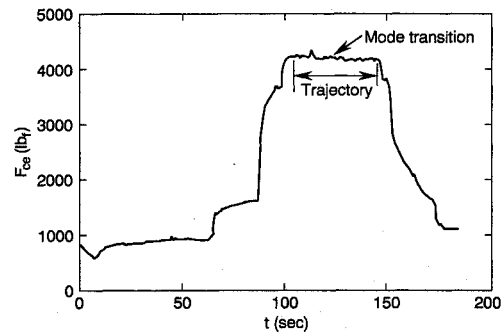

Fig. 14 Measured combustor exit stream thrust during transition.

continued to move downstream. Two additional pressure spikes are seen, one at $t = 122$ s and $t = 127$ s. The first spike is indicative of the transient nature of the shock structure. The second spike appears to be caused by the small oscillation in fuel flow (see Fig. 11).

Figure 12c is a pressure trace downstream of the fuel injection. This is in a short ($L = 3$ in.) constant area section downstream of the injectors; therefore, there is no thrust produced at this location. The pressure trace is similar to Fig. 12b, again indicating the unsteady behavior of the transition process.

Figure 12d is a trace well downstream of the fuel injection and is in the diverging section (i.e., thrust producing). The unsteadiness of the shock system can still be seen; however, the effect is very small. Essentially, the pressure dropped steadily during the acceleration, due to the decreased fuel flow rate.

The effect of the transition process can be seen more clearly by plotting the pressure through the combustor (see Fig. 13). The analysis software was set up for steady-state tests, and therefore, the data was averaged over a 2-s time period. Even though the results are an average of transient data, the movement of the shock system is evident. The shock system at the beginning of the trajectory was clearly located upstream of the fuel injection station with peak pressures reaching $P \approx 43$ psia. Between $t = 120$–125 s the shock system moved considerably downstream. For $t = 144$–146 s the peak pressure was $P \approx 20$ psia which is below the separation pressure ($P_{sep} \approx 27$ psia); hence, the shock system was eliminated. This transition occurred at a simulated Mach number of $M \approx 5.95$ ($T_t \approx 2800$°R).

Bearing in mind that the traces in Fig. 13 are based on an average of transient data, they can still be compared to those in Fig. 8, which are based on steady-state tests. The peak pressures are somewhat different for the two cases, due to the averaging process; however, the trends are similar between the steady-state and transient results. Before performing the tests, a primary concern was that once the flowfield was separated, it might remain separated for the entire trajectory, delaying mode transition; however, this did not occur.

In Fig. 13, the pressure trace prior to transition shows a rapid decrease in pressure at the shoulder of the diverging section. After transition occurred, the pressure decrease downstream of the shoulder was more gradual; in fact, before and after transition, there is very little difference in the pressure traces. The combustor thrust ($F_4 - F_2$) decreases approximately 7% during the acceleration; however, the combustor entrance stream thrust increased by almost the same amount which caused the combustor exit stream thrust to remain nearly constant (see Fig. 14). During the transition ($t = 120$–125 s) there was some unsteadiness in the trace, but there was no appreciable drop in combustor thrust at the transition point. This was surprising considering the difference in the peak pressure before and after transition.

Summary

A facility has been established to investigate the performance of a hydrogen-fueled scramjet combustor. The facility uses a combustion heater to elevate the air temperature to between $T_t = 1000$–4200°R. A computer-controlled system is utilized to control the flow rate of the various gases (air, H_2, and O_2) to the heater. The use of this control system allows the gases to be varied in a predetermined manner to change the inflow conditions (simulated flight Mach number based on enthalpy) to the combustor.

A demonstration was performed in which the combustor entrance temperature was varied from $T_t = 2720$–3070°R, simulating a vehicle acceleration between $M = 5.85$–6.2. This was not a limiting range but was chosen in anticipation of a significant transition in the mode of operation of the combustor. The combustor fuel flow rate was decreased during the acceleration in order to maintain a constant equivalence ratio.

The pressure rise in the combustor initially created a separation of the boundary layer, and subsequently a precombustion shock system formed. As the simulated acceleration progressed, the pressure rise in the combustor decreased to below the separation pressure and the precombustion shock system was eliminated. This appears to be a very unsteady process, and small deviations in fuel flow significantly affect the movement of the shock train.

In the diverging combustor, where the thrust is produced, the effect of the shock movement and transition is reduced significantly. The combustor thrust decreased gradually (7%) during the acceleration; however, there was no step decrease in the thrust at the onset of transition even though the peak pressure is reduced by one-half at the higher Mach number simulation.

References

[1]Curran, E. T., Leingang, J. L., and Donaldson, W. A., "Review of High Speed Air Breathing Propulsion Systems," *Proceedings of the Eighth International Symposium on Air Breathing Engines*, AIAA, Washington, DC, June 1987.

[2]Waltrup, P. J., and Billig, F. S., "Structure of Shock Waves in Cylindrical Ducts," *AIAA Journal*, Vol. 11, No. 10, 1973, pp 1404–1408.

[3]Stockbridge, R. D., "Experimental Investigation of Shock Wave/Boundary Layer Interactions in Annular Duct," *AIAA Journal of Propulsion and Power*, Vol. 5, No. 3, 1989, pp 346–352.

[4]Bement, D. A., Stevens, J. R., and Thompson, M. W., "Measured Operating Characteristics of a Rectangular Combustor/Inlet Isolator," AIAA Paper 90-2221, July 1990.

[5]Billig, F. S., Corda, S., and Pandolfini, P. P., "Design Techniques for Dual Mode Ram-Scramjet Combustors," AGARD 75th Symposium on Hypersonic Combined Cycle Propulsion, AGARD-CP-479, Paper 23, Madrid, Spain, May 28–June 1, 1990.